Icarus 224 (2013) 286–296

Contents lists available at SciVerse ScienceDirect

Icarus

journal homepage: www.elsevier.com/locate/icarus

Geochemistry of a continental site of serpentinization, the Tablelands Ophiolite, Gros Morne National Park: A Mars analogue

Natalie Szponar [a], William J. Brazelton [b], Matthew O. Schrenk [b], Dina M. Bower [c], Andrew Steele [c], Penny L. Morrill [a,*]

[a] Department of Earth Sciences, Memorial University of Newfoundland, 300 Prince Philip Dr., St. John's, NL, A1C 3W8, Canada
[b] Department of Biology, East Carolina University, Greenville, NC 27858, USA
[c] Geophysical Laboratory, Carnegie Institution for Science, 5251 Broad Branch Rd., Washington, DC 20015, USA

ARTICLE INFO

Article history:
Available online 16 July 2012

Keywords:
Earth
Mars
Astrobiology
Geological processes

ABSTRACT

The presence of aqueously altered, olivine-rich rocks along with carbonate on Mars suggest that serpentinization may have occurred in the past and may be occurring presently in the subsurface, and possibly contributing methane (CH_4) to the martian atmosphere. Serpentinization, the hydration of olivine in ultramafic rocks, yields ultra-basic fluids (pH $\geqslant$ 10) with unique chemistry (i.e. Ca^{2+}–OH^- waters) and hydrogen gas, which can support abiogenic production of hydrocarbons (i.e. Fischer–Tropsch Type synthesis) and subsurface chemosynthetic metabolisms. Mars analogue sites of present-day serpentinization can be used to determine what geochemical measurements are required for determining the source methane at sites of serpentinization on Earth and possibly on Mars. The Tablelands Ophiolite is a continental site of present-day serpentinization and a Mars analogue due to the presence of altered olivine-rich ultramafic rocks with both carbonate and serpentine signatures. This study describes the geochemical indicators of present-day serpentinization as evidenced by meteoric ultra-basic reducing groundwater discharging from ultramafic rocks, and travertine and calcium carbonate sediment, which form at the discharge points of the springs. Dissolved hydrogen concentrations (0.06–1.20 mg/L) and methane (0.04–0.30 mg/L) with $\delta^{13}C_{CH4}$ values (−28.5‰ to −15.6‰) were measured in the spring fluids. Molecular and isotopic analyses of CH_4, ethane, propane, butane, pentane and hexane suggest a non-microbial source of methane, and attribute the origin of methane and higher hydrocarbon gases to either thermogenic or abiogenic pathways.

1. Introduction

The detection of methane (CH_4) and its short lifetime in the martian atmosphere (Formisano et al., 2004; Krasnopolsky et al., 2004; Mumma et al., 2009), has led to much discussion regarding the source of methane on Mars. A possible source of methane has been attributed to serpentinization, a fluid–rock reaction common in ultramafic rocks that has been hypothesized to occur on Mars (Boston et al., 1992; Formisano et al., 2004; Atreya et al., 2007; Oze and Sharma, 2007). This reaction produces hydrogen (H_2) and the reducing conditions necessary for abiogenic hydrocarbon synthesis through the hydration of ultramafic rock, while also producing conditions for the production of methane through chemolithoautotrophic pathways. On Earth, serpentinization has been observed in ultramafic rocks on the sea floor at deep sea hydrothermal vents such as the Lost City hydrothermal field (Kelley et al., 2005), and on continents in ophiolites (Barnes et al., 1978; Abrajano et al., 1990; Blank et al., 2009; Etiope et al., 2011). Ophiolites are sections of the ocean crust and upper mantle that have been obducted onto continental crust that can yield ground waters with unique chemistry that are ultra-basic (pH > 10), and/or Ca^{2+}–OH^- rich (Barnes et al., 1967). The Tablelands Ophiolite (also referred to in literature as the Bay of Islands Ophiolite) in Gros Morne National Park, Newfoundland, Canada is a continental site exhibiting present-day serpentinization. Olivine-rich ultramafic rocks, prerequisites for serpentinization, have been found on Mars (Hoefen et al., 2003; Hamilton and Christensen, 2005; Quesnel et al., 2009; Ehlmann et al., 2010), and also occur at the Tablelands massif, thus making the Tablelands Ophiolite an important terrestrial analog for Mars.

During serpentinization, ultramafic rocks composed of mostly olivine [$(Mg,Fe)_2SiO_4$] and pyroxene [orthopyroxene (Mg,Fe)–SiO_3 and clinopyroxenes $Ca(Mg,Fe)Si_2O_6$] undergo hydration producing serpentine (Eq. (1)). In a half reaction, iron hydroxide, which is produced via hydration of the iron-endmember of olivine, undergoes subsequent oxidation of Fe^{2+} and produces magnetite and hydrogen gas (Eq. (2)). The hydration of olivine and clinopyroxenes also releases OH^- ions resulting in highly alkaline fluids, which can emerge from fractures in the ultramafic rocks (Coleman and Keith,

* Corresponding author. Fax: +1 709 864 2589.
E-mail address: pmorrill@mun.ca (P.L. Morrill).

0019-1035/$ - see front matter © 2012 Elsevier Inc. All rights reserved.
http://dx.doi.org/10.1016/j.icarus.2012.07.004

1971). Under basic conditions and in the presence of inorganic carbon, Ca^{2+} and Mg^{2+} form calcium and magnesium carbonate respectively (Eqs. (3) and (4)).

$$\underset{faylite}{3Fe_2SiO_4} + \underset{forsterite}{5Mg_2SiO_4} + 9H_2O \rightarrow \underset{serpentine}{3Mg_3Si_2O_5(OH)_4} + \underset{bructite}{Mg(OH)_2} + \underset{iron(II)hydroxide}{2Fe(OH)_2} \quad (1)$$

$$3Fe(OH)_2 \rightarrow \underset{magnetite}{Fe_3O_4} + 2H_2O + H_2 \quad (2)$$

$$Ca^{2+} + CO_3^{2-} \rightarrow \underset{calcium\ carbonate}{CaCO_{3(s)}} \quad (3)$$

$$Mg^{2+} + 2HCO_3^- \rightarrow \underset{magnesium\ carbonate}{MgCO_{3(s)}} + CO_2 + H_2O \quad (4)$$

The production of hydrogen gas results in conditions capable of reducing dissolved inorganic carbon species and forming abiogenic hydrocarbons (Sleep et al., 2004). In the following generalized reaction for abiogenic hydrocarbon formation (i.e. the Fischer Tropsch Type synthesis) (Schulz, 1999), H_2 gas reduces inorganic carbon to form methane and other higher molecular weight hydrocarbon gases:

$$CO_2 + H_2 \rightarrow CH_4 + C_2H_6 + C_3H_8 + C_nH_n \ldots + H_2O \quad (5)$$

In addition to abiogenic hydrocarbons, the ultra-basic reducing groundwaters associated with active serpentinization sites are suitable niches for microorganisms that can tolerate high pH environments with anaerobic microbial metabolisms including those of hydrogen-utilizing microbes, such as homoacetogens and methanogens (Kelley et al., 2005; Brazelton et al., 2006; Schulte et al., 2006). Therefore, sites of serpentinization may support the production of either abiogenic hydrocarbons or microbial methane or both. Apart from abiogenic and microbial synthesis, hydrocarbons can form by the thermal decomposition of sedimentary organic matter (thermogenic hydrocarbons). Gaseous hydrocarbons produced through the thermal alteration of sedimentary organic matter underlying an ophiolite complex may migrate to the surface through the highly fractured weathered ultramafics. The Tablelands Ophiolite formed during the closure of the Iapetus Ocean and the collision of Laurentia and Gondwana continents approximately 485 myr ago (Elthon, 1991). Underlying ultramafic rocks of the Earth's mantle were obducted onto the continental margin of Laurentia, deforming and trapping clastic sedimentary rocks and limestones underneath the ophiolite complex through folding and faulting (Elthon, 1991). The possible thermal alteration of the sedimentary organic matter could produce hydrocarbon gases. Therefore, thermogenic hydrocarbons may also be present at the Tablelands.

Ultra-basic reducing springs have been identified in the Tablelands Ophiolite (Stevens, 1988). One of the main objectives of this study is to determine if these springs contain H_2, CH_4 and other hydrocarbons. Highly reducing conditions and the detection of H_2 in ground waters discharging from the Tablelands may provide conditions amenable for either abiogenic and/or biogenic production of CH_4 and subsequently other higher molecular weight hydrocarbons.

The process of serpentinization is of particular interest for the exploration of Mars and determining the origin of CH_4. Serpentinization leaves mineralogical evidence of a previous physicochemical environment that would provide conditions for the production of methane and potentially other hydrocarbon gases to the martian atmosphere (Schulte et al., 2006). Near-infrared data from orbiting imaging spectrometer MRO-CRISM have shown the presence of Mg carbonate and serpentine signatures in several outcrops on Mars, suggesting that serpentinization occurred in the past and was active at least >3–7 Gyr ago (i.e. Noachian) (Ehlmann et al., 2008, 2010). Similarities in the martian crust to terrestrial ophiolites, and the lack of significant tectonic activity suggest that serpentinization would occur in localized areas where there is active fluid flow, potentially in the subsurface (Schulte et al., 2006; Vance et al., 2007). Orbital reconnaissance data has identified water ice extant in the subsurface, and the possible flows of liquid water (likely saline brines) in the upper martian regolith (Holt et al., 2008; McEwen, 2011). The presence of fluvial channels and water-forming minerals such as carbonates, phyllosilicates, and sulfates within the martian's crust support the potential for the process to be active in the past (Mustard et al., 2008; Boynton et al., 2009; Quesnel et al., 2009; Niles et al., 2010). However, if subsurface water on Mars is extant and in contact with ultramafic rocks, then serpentinization may still be occurring (Ehlmann et al., 2010).

Two possible source regions: Nili Fossae and North Eastern Syrtis have been found where both reactants (olivine) and products (serpentine, carbonates) of serpentinization are present (Ehlmann et al., 2010). Methane measured at these source regions would require either recent serpentinization, where active fluid flows would be in contact with ultramafics, such as in the subsurface; or be the result of Noachian serpentinization, where methane would likely have been trapped for billions of years. The presence of methane clathrates reservoirs in the martian subsurface and/or polar ice caps would allow for the storage and slow release of methane to the atmosphere (Max and Clifford, 2000; Chastain, 2007). A solid understanding of the mineralogy and geochemistry associated with serpentinization is necessary for locating and sourcing methane on Mars. Terrestrial sites of serpentinization can be used to investigate the geochemical measurements required for understanding the serpentinization process, and determine sources and reaction pathways that could be responsible for the methane detected in the martian atmosphere.

The Gale Crater, the landing site for the Mars Sample Laboratory (MSL) is interpreted as an ancient lake, which will likely provide context for Mars geological history, but not insight into the minerals associated with serpentinization that have been observed on the basis of the CRISM data. However, the Sample Analysis at Mars (SAM) investigation on the MSL will conduct *in situ* surveys of gases such as methane in the martian atmosphere to localize and understand the nature of their production (Mahaffy, 2008, 2012).

The aim of this study is to present characteristic aqueous geochemistry, carbonate mineralogy, and hydrocarbon source signatures associated with present-day serpentinization occurring at the Tablelands Ophiolite in Gros Morne National Park, Newfoundland, Canada, in attempt to provide geochemical parameters relevant for planning future Mars exploration missions.

2. Material and methods

2.1. Site description

Highly reducing, ultra-basic springs discharging from serpentinized peridotite (i.e. harzburgite with some lherzolites) (Suen et al., 1979) rocks were located in the Tablelands Ophiolite in Gros Morne National Park (N49°27′58.9″, W57°57′29.0″) (Fig. 1). The spring fluids are Ca^{2+}–OH^- type waters similar to those described by Barnes and O'Neil (Barnes et al., 1967). Inorganic carbon precipitates in these waters and is found as either carbonate sediment, travertine, or conglomerate cements that form where the springs discharge. Three sampling locations were identified on the northeastern face of the Tablelands and within Winter House Canyon: Wallace Brook (WB), Tablelands East (TLE), and Winter House Canyon (WHC) are shown in Fig. 2. TLE and WB were located on the slope of the Tablelands massif with travertine deposits and discharging Ca^{2+}–OH^- type waters. Located in WHC is a pool of ultra-basic water (labeled WHC2) that is approximately 40 cm

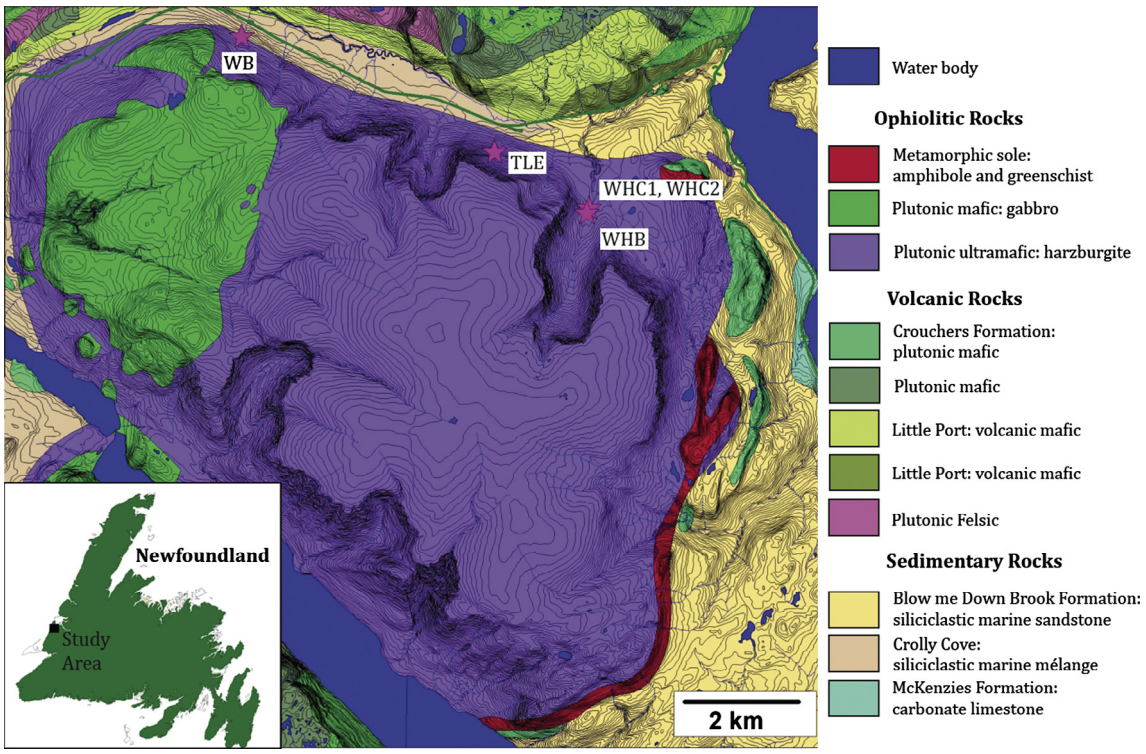

Fig. 1. Geologic map, modified from (Berger et al., 1992), showing the Tablelands massif and approximate sampling locations (star symbols): Wallace Brook (WB), Tablelands East (TLE), Winterhouse Creek (WHC1, 2a, b, c); and Winterhouse Brook (WHB). The Tablelands is located in Gros Morne National Park in Newfoundland, Eastern Canada.

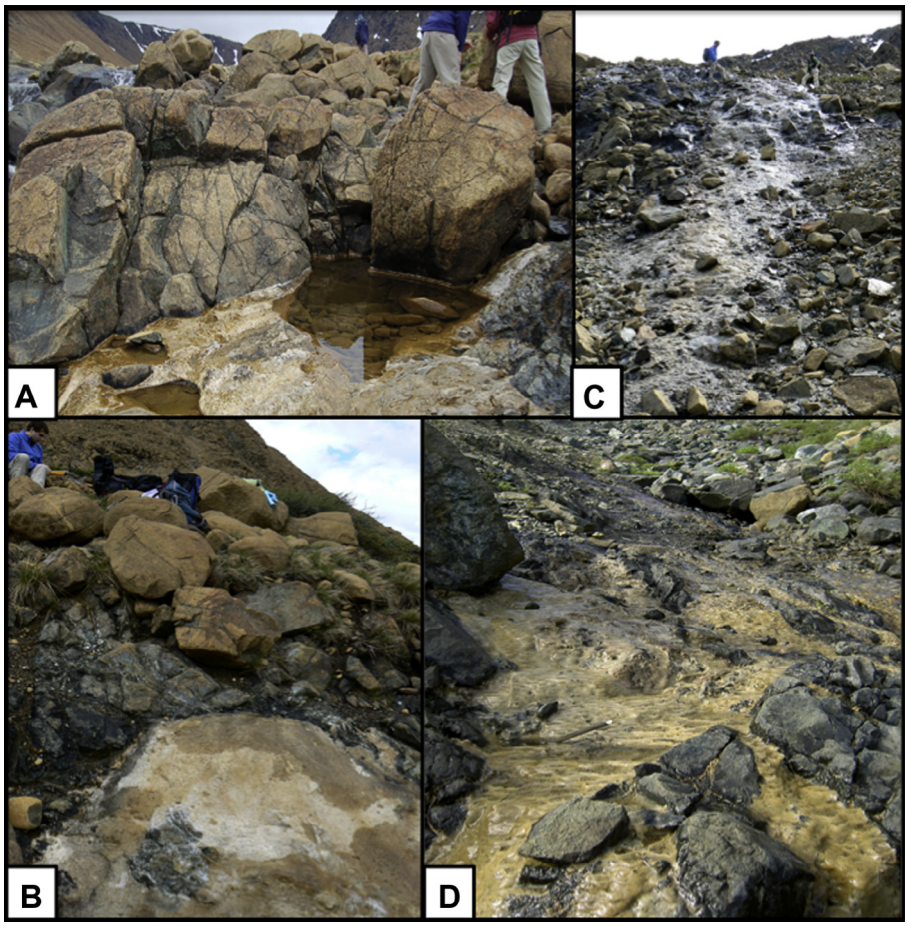

Fig. 2. Images of springs and travertine deposits at sampling locations: (A) Winterhouse Creek 1 (2a, human for scale ~1.70 m); (B) Winterhouse Creek 2 (2b, human for scale ~1.70 m); (C) Tablelands East (2c, human for scale ~1.70 m); and (D) Wallace Brook (2d, spatula for scale ~22 cm).

deep and 126 cm wide, and exposed to the atmosphere at the surface. A survey of the bottom of WHC2 pool using handheld pH and Eh meters showed that there were two distinct locations where the pH was the highest and the Eh was the lowest indicating that there are two ultra-basic, reducing spring discharge points at the bottom of WHC2 (labeled WHC2a and WHC2b). A third sampling location (WHC2c) was selected for this study. At this location freshwater from overland flow trickles into the WHC2 pool. This site was of particular interest for studying the geochemical and biological interactions at a mixing site with large redox and nutrient gradients. The carbonate sediment at the bottom of the WHC2, and the travertine on the side of WHC2 spring were also sampled to determine the source of the inorganic carbon. A small and shallow oval shaped pool (approximately 2 cm deep, 5 cm wide) of ultra-basic spring water seeping from the travertine deposit was located approximately a meter from WHC2. It is identified as WHC1. WHC1 discharges at rate of 1 mL/min, and its surface is continuously exposed to the atmosphere; however, this pool was continuously flushed with ultra-basic groundwater and no freshwater inputs to WHC1 were indentified. Winter House Brook (WHB) which flows along the bottom of Winter House Canyon was identified as the freshwater end member.

2.2. Aqueous geochemistry sampling and analysis

Daily field measurements of pH and redox potential (E_h) were obtained during sampling trips in July and September, 2009; June, August, and October, 2010; and June, 2011. Redox and pH values of water samples were measured using an ORPTestr 10 m (Eutech Instruments), pH paper and handheld pH meter (IQ Scientific Instruments GLP series IQ180G) respectively. Redox and pH values were measured during sampling to identify any changes in these parameters during or after water sampling, and after rainfall events. Samples were collected at least 48 h following a rainfall event to minimize dilution effects.

Samples for total inorganic carbon (TIC) and dissolved organic carbon (DOC) were collected for both concentration and stable carbon isotope ($\delta^{13}C$) values in pre-combusted 40 mL amber vials spiked with mercuric chloride ($HgCl_2$) and phosphoric acid (H_3PO_4) respectively. Samples for DOC were filtered through a 0.7 μm pre-combusted glass microfiber filter. TIC and DOC concentrations and $\delta^{13}C$ values were determined using an OI Analytical Aurora 1030 TOC Analyzer equipped with a reduction furnace, water trap, and packed GC column; coupled to a ThermoElectron DeltaVPlus Isotope Ratio Mass Spectrometer (IRMS) system via a Conflo III interface or a Finnigan MAT252 IRMS. The Aurora uses a wet chemical oxidation process to extract carbon as CO_2 gas using phosphoric acid for total inorganic carbon (TIC) and Na-persulfate for total dissolved organic carbon (DOC). Accuracy and reproducibility for concentration was ±1.5% RSD and ±0.5‰ for $\delta^{13}C$. $\delta^{13}C$ values are reported in delta notation relative to the Vienna Pee Dee Belemnite (PDB) reference standard.

Water samples were collected for hydrogen and oxygen isotopes (δD_{H2O}, $\delta^{18}O_{H2O}$) in pre-combusted 4 mL vials with no headspace. Oxygen and hydrogen measurements were analyzed at Isotope Tracer Technologies in Waterloo, Ontario on a Picarro Cavity Ring Down Spectroscopy Analyzer (Model L1102-*i*). Precision on multiple $\delta^{18}O$ and δD measurements was ±0.1‰ and ±0.6‰ respectively. All results for oxygen and hydrogen are reported in delta notation relative to the Vienna Standard Mean Ocean Water (SMOW) reference standard.

Water samples were collected for major-ions chemistry and measured on an inductively coupled plasma mass spectrometer (ICP-MS) at Memorial University of Newfoundland using an ELAN DRCII ICP-MS. Samples for ICP-MS were filtered through a 0.45 μm filter and collected in 125 mL Trace-Clean bottles and immediately acidified with 5 N nitric acid. Certified reference materials were used for quality control. The detection limit on conservative ions Cl^- was <0.01 mg/L, and <1.7 mg/L for Br^-. The detection limit on Ca^{2+} and Mg^{2+} were <167 μg/L and <0.35 μg/L respectively. Total analytical error was ±10% RSD.

2.3. Carbonate mineralogy and isotope analysis

Samples of travertine and carbonate sediment from spring locations were collected for trace element geochemistry, carbon ($\delta^{13}C$) and oxygen ($\delta^{18}O$) isotopes. Samples were frozen upon collection, freeze dried, and ground to a fine powder with a mortar and pestle. X-ray diffraction was employed on powdered carbonates to determine measurements of major minerals present.

$\delta^{13}C$ and $\delta^{18}O$ isotopes of carbonates were analyzed using a ThermoElectron Gas Bench II interfaced to an IRMS. Samples were measured into glass vials, placed in a heated block (50 °C), and flushed with helium prior to injection with phosphoric acid. The resultant gases were passed through Nafion dryers and a capillary column prior to entering into an ion source. External calcium carbonate standards CBM, NBS-19, and SPEX were used. Accuracy and reproducibility on $\delta^{18}O$ and $\delta^{13}C$ measurements was ±0.1‰ and ±0.5‰, and reported in delta notation relative to SMOW and PDB standards respectively.

2.3.1. Dissolved gas sampling

Dissolved gases including: H_2; CH_4; and other hydrocarbons including: ethane (C_2H_6, C_2), propane (C_3H_8, C_3), butane (C_4H_{10}, C_4), pentane (C_5H_{12}, C_5), and hexane (C_6H_{14}, C_6) were sampled using a modified syringe gas phase equilibration technique by McAuliffe (1971) and Rudd et al. (1974). Twenty milliliters of fluid was withdrawn with a 60 mL sterile syringe and shaken vigorously for 5 min with an equal volume of helium (He). This allowed for partitioning of the dissolved gas in the sample water into to the gas phase. The entire gas phase of 2 syringes (40 mL) was injected into a 30 mL serum vial, prefilled with degassed water and sealed with blue butyl stoppers. The dissolved gases in He displaced the water in the serum vial. Samples were collected in triplicates for most sampling periods. The samples that were not sampled in triplicate were at least sampled in duplicate. Samples were fixed with 5 μL-saturated solution of $HgCl_2$ to ensure there was no microbial growth in bottles.

Dissolved gases were sampled for $\delta^{13}C$ analysis by collecting 50 mL of fluid using a 60 mL sterile syringe and injecting samples into a pre-evacuated 125 mL serum vial fixed with $HgCl_2$ and sealed with blue butyl stoppers. Samples were collected in triplicate.

2.3.2. Analysis of dissolved gases

Dissolved gases including H_2 and CH_4 were analyzed for concentration using a portable SRI 8610 Gas Chromatograph (GC) with a Thermal Conductivity Detector (TCD) and a Flame Ionization Detector (FID). The gases were separated using a Carboxen 1000 column packed in stainless steel (15 ft × 1/8 in., 2.1 mm film thickness) with a temperature program: 35 °C, hold 5 min, ramp at 20 °C/min to 225 °C, hold 15 min with a He carrier gas. Hydrocarbons were also analyzed by a GC equipped with a FID on a Porabond-Q column (30 m × 0.25 mm, 0.25 μm film thickness) with a temperature program of 35 °C hold 8 min, 10 °C/min to 150 °C, hold 8 min, ramp 5 °C/min to 210 °C, hold 10 min. Reproducibility on replicate samples was better than 5%.

Stable carbon isotope ratios of CH_4 were measured using an Agilent 6890 GC equipped with the Carboxen 1010 column coupled to a Finnigan MAT252 IRMS via combustion Conflo II Interface (GC-C-IRMS). Methane isotopes were determined using a 5:1 split ratio and a 100 °C isothermal temperature program. Low molecular weight hydrocarbons (C_2, C_3, iC_4, nC_4, iC_5, nC_5, C_6) were determined

on the Porabond Q column using a 5:1 split ratio and the same temperature program as used for concentration analysis.

Samples were withdrawn from serum bottles and injected directly into the GC-C-IRMS system. On each injection onto the Carboxen 1010 column, $\delta^{13}C$ of CH_4 was determined. On each injection onto the Porabond-Q column, $\delta^{13}C$ of low molecular weight hydrocarbons was determined. All results are reported in delta notation relative to the PDB standard reference material. Accuracy and reproducibility for $\delta^{13}C$ were ±0.5‰. This error incorporates both internal reproducibility on triplicate measurements and accuracy of instrumental measurement of a standard with a known isotopic value.

All isotope ratios are reported in delta notation (e.g. $\delta^{13}C$, ^{18}O, δD) relative to an international standard (e.g. V-PDB, SMOW) using:

$$\delta\ (‰) = (R_{sample}/R_{standard} - 1) \times 1000 \quad (6)$$

where R is the ratio of heavy to light isotopes.

3. Results and discussion

3.1. Origin of spring water

The δD_{H2O} and $\delta^{18}O_{H2O}$ of the ultra-basic springs and freshwater including WHB, snowmelt, rainwater, and surface pond water collected from the top of the Tablelands massif plot close to the global meteoric water line (GMWL) (Fig. 3a), indicating that the ultra-basic spring fluids are meteoric in origin. This further suggests that the groundwater discharging from the peridotite rocks has been in recent contact with the atmosphere, excluding connate water or magmatic water sources.

The GMWL is representative of precipitation data collected from different locations globally as determined by (Craig, 1961) and therefore represents the global relationship between δD_{H2O} and $\delta^{18}O_{H2O}$. The δD_{H2O} and $\delta^{18}O_{H2O}$ data from the Tablelands do not plot directly on GMWL, which likely reflects the local conditions that control the δD_{H2O} and $\delta^{18}O_{H2O}$ relationship. A linear line of regression representing the freshwater sources was added to Fig. 3a as a proxy of the local meteoric water line (LMWL) for the Tablelands. δD_{H2O} and $\delta^{18}O_{H2O}$ of spring fluids plot closely to the LMWL indicating a similar δD_{H2O} and $\delta^{18}O_{H2O}$ relationship as the freshwater. Therefore, changes in local meteoric conditions (e.g. temperature) likely govern the δD_{H2O} and $\delta^{18}O_{H2O}$ of freshwater and ultra-basic springs respectively.

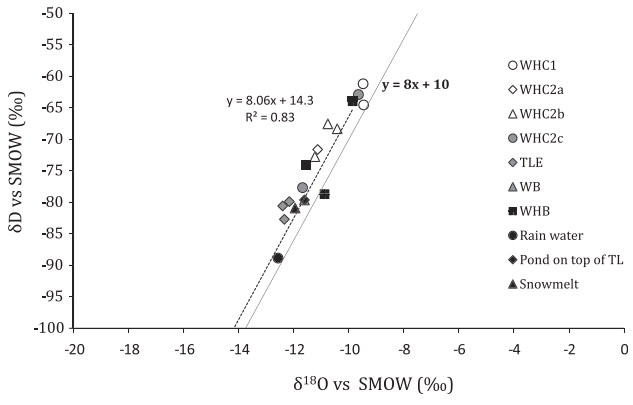

Fig. 3a. $\delta^{18}O$ and δD of fluids sampled from all sites including rainwater, snowmelt, and pond water collected from the top of the Tablelands. $\delta^{18}O$ and δD of fluids are plotted with the GMWL (solid line) and the linear regression for collected freshwater as a proxy for the LMWL (dashed line). Error on $\delta^{18}O$ and δD represent ±0.1‰ and ±0.6‰ respectively. Note that error bars are smaller than the plotted symbol.

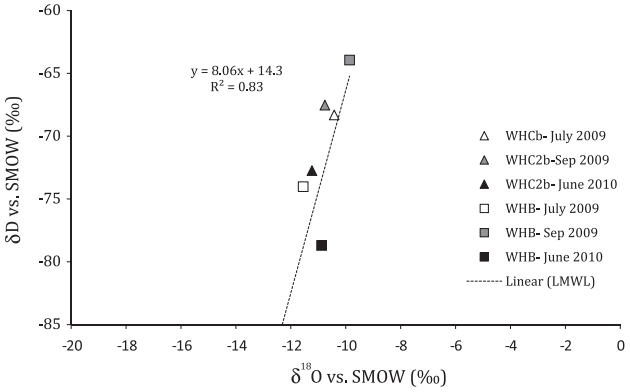

Fig. 3b. $\delta^{18}O$ and δD of waters sampled from WHC2b and WHB during different seasons: July and September 2009, and June 2010.

Fractionation of D_{H2O} and $^{18}O_{H2O}$ is a function of temperature, with a greater fractionation associated with decreasing temperatures, resulting in a depletion of D_{H2O} and $^{18}O_{H2O}$. Samples were collected over different seasons with varying temperatures. A seasonal trend related to temperature was observed in both spring fluids (WHC2b) and freshwater with an isotopic depletion during colder seasons and enrichment during warmer seasons (WHB) (Fig. 3b). The most isotopically depleted D_{H2O} and $^{18}O_{H2O}$ were observed in early June (winter–spring season), when there was snow cover on the Tablelands and colder surface temperatures. The most enriched D_{H2O} and $^{18}O_{H2O}$ were observed in September (summer–fall season) when there was no snow cover and warmer surface temperatures.

3.2. Mixing of freshwater and ultra-basic fluids at springs

In order to better understand changes in geochemical parameters in the springs, the contributions of freshwater and ultra-basic fluids were quantified at sites where mixing of the two end members was suspected. Fig. 4 represents a conservative 2-component mixing model between the freshwater end member (represented by WHB) and the ultra-basic reducing end member (represented by WHC1). In this model bromine (Br^-) and chlorine (Cl^-) are assumed to be conservative tracers of these two end members. The data from WHC2a, WHC2b, and WHC2c are well represented by the model and therefore suggest that the Cl^- or Br^- concentrations

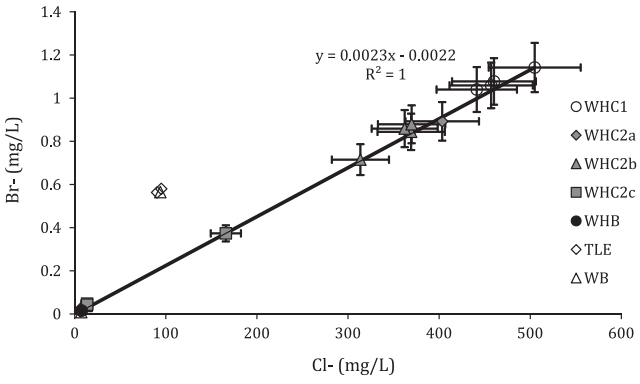

Fig. 4. Dissolved ion concentrations of Br^- and Cl^- as conservative tracers to determine mixing of freshwater and ultra basic water. Samples plotted are from WHC1, WHC2a, WHC2b, WHC2c, TLE, WB, and WHB collected in September 2009 and June 2010. The solid line represents conservative mixing between the freshwater (WHB) and ultra basic (WHC1) end member. Note that TLE and WB do not plot on the conservative mixing line. Error bars are ±10% for Br^- and Cl^- and may appear smaller than the plotted symbol.

Table 1
A comparison of average (±std, 1σ) aqueous geochemical parameters of spring waters.

	Freshwater endmember	Mixing springs with freshwater inputs					Ultra-basic endmember
	WHB	TLE	WB	WHC2c	WHC2b	WHC2a	WHC1
pH	7.6 (±0.7)	10.6 (±0.5)	10.7 (±0.2)	11.8 (±0.8)	12.3 (±0.3)	12.3 (±0.3)	12.2 (±0.2)
Eh (mv)	415 (±26)	186 (±55)	318 (±64)	−437 (±229)	−552 (±103)	−609 (±118)	121 (±12)
Cl^- (mg/L)	3.7 (±0.23)	49 (±61)	50 (±61)	166 (±17)	340 (±38)	403 (±40)	479 (±37)
Br^- (mg/L)	0.009 (±0.002)	0.29 (±0.39)	0.29 (±0.39)	0.37 (±0.04)	0.79 (±0.1)	0.89 (±0.09)	1.1 (±0.06)
Mg^{2+} (mg/L)	13.3 (±1.3)	1.12 (±0.4)	1.47 (±0.05)	7.57 (±0.4)	1.12 (±0.7)	0.61 (±0.1)	0.06 (±0.01)
Ca^{2+}/Mg^{2+}	0.08 (±0.01)	29 (±18)	23 (±20)	3 (±0.3)	57 (±42)	97 (±9.0)	144 (±5.0)
TIC (mg/L)	8.06 (±1.7)	0.83 (±0.5)	0.8 (±1.0)	14.9 (±2.5)	4.45 (±6.3)	1.1 (±0.5)	27.25 (±15)
TIC $\delta^{13}C$ ‰	−1.7 (±0.8)	−11.4 (±2.4)	−18.6 (±3.0)	−12.5 (±0.8)	−16.2 (±3.0)	−15.2 (±2.9)	−29.4 (±1.7)
DOC (mg/L)	0.46 (±0.2)	0.16 (±0.1)	0.19 (±0.1)	1.24 (±0.4)	0.96 (±0.6)	1.62 (±1.0)	2.04 (±0.6)
DOC $\delta^{13}C$ ‰	−27.1 (±0.6)	−23.3 (±0.5)	<d.l.	−23.7 (±1.5)	−22.1 (±6.0)	−17.7 (±1.8)	−18.2 (±1.1)

<d.l. = less than detection limit.

can be used to calculate the fraction of ultra-basic water (f_{UB}) contributing to the mixing sites (WHC2a, WHC2b, WHC2c). Sampling sites that are farther away from WHB and WHC (i.e. TLE and WB), are not as well described by the mixing model. This could be due to differences in the geochemistry of the end members for the TLE and WB springs. Likewise, TLE and WB, which are located on a steep slope of the Tablelands massif, received water inputs in the form of surface runoff, which could contribute to large differences observed in aqueous geochemistry seasonally, and account for larger standard deviations (Table 1).

Average measurements of pH, redox, and dissolved gas composition of fluids from the Tablelands can be seen in Table 1. Standard deviations reflect seasonal and annual variability in the geochemical parameters. The highest pH measurements were found at WHC1 (12.2), WHC2a (12.3), and WHC2b (12.3). Redox measurements remained consistently low at WHC2a and WHC2b (−552 to −609 mV) at the bottom of the WHC pool where a distinct anoxic zone was observed. Higher redox values (+415 mV) were measured for the more oxidizing WHB freshwater end member. The redox value of the groundwater spring discharging at WHC1 increased during sampling. This occurred because of the slow recharge rate of the seep and exposure to the atmosphere, which allowed for atmospheric O_2 to partition into spring water and increase the redox value while sampling. Redox measurements where higher at mixing spring locations with oxygen-containing freshwater inputs (i.e. WHC2c, TLE, and WB). Differences in redox measurements reflect different amounts of mixing of freshwater and ultra-basic water at different times of sampling.

3.3. Geochemical evidence of present-day serpentinization

Fluids found discharging from serpentinized peridotites at the Tablelands Ophiolite are geochemically distinct from freshwater as evidenced by high pH, negative redox potentials, and the presence of H_2.

Dissolved H_2 concentrations were the highest (1.04 and 1.18 mg/L) at the most reducing sites with the least amount of mixing with freshwater and minimum exposure to the atmosphere (WHC2a and WHC2b). Lesser amounts of dissolved hydrogen (0.57–0.36 mg/L) were measured at sites with greater mixing between the ultra-basic reducing groundwater and the surface freshwater (WHC2c, TLE) and at slow discharging sites where the ultra-basic groundwater was directly exposed to the atmosphere for at least 10 min before sampling could occur (WHC1). During this time frame, dissolved hydrogen gas may have been released to the atmosphere. Dissolved hydrogen gas measurements were below detection at WB.

Likewise, major trace elements Mg^{2+} and Ca^{2+}, derived from the hydration of olivine and clinopyroxenes respectively, are often found in fluids discharging from serpentinized ultramafic rocks giving evidence for active serpentinization. High Ca^{2+}/Mg^{2+} are found in the ultra-basic springs at continental sites of serpentinziation such as Cazadero in California (Barnes et al., 1967). Through serpentinization, soluble Mg^{2+} concentrations become accommodated into serpentine and soluble Ca^{2+} gets released into the water. Therefore, higher ratios of Ca^{2+} to Mg^{2+} are observed. Similarly, high Ca^{2+}/Mg^{2+} ratios were found in the ultra-basic springs at the Tablelands (see Table 1).

In Fig. 5, Ca^{2+}/Mg^{2+} ratios from spring fluids at WHC2a, WHC2b, and WHC2c at certain sampling periods are well described by the 2-component conservative mixing model defined from the freshwater and ultra-basic end members. The highest Ca^{2+}/Mg^{2+} ratios are observed at most ultra-basic springs, similar to those observed in the Cazadero, CA ultra-basic springs. Ca^{2+}/Mg^{2+} ratios were observed at WHC2b (f_{UB} = 0.62) and WHC2c (f_{UB} = 0.32) are not well described by the 2-component model. A possible third end member rich in Mg^{2+}—HCO_3^- may be contributing to the spring fluids. As described by Barnes et al. (1967), Mg^{2+}—HCO_3^- rich fluids can be found in localities of incomplete or inactive serpentinization resulting in shallow, moderately basic groundwater that is related to the weathering of serpentine and other magnesium-bearing minerals. High Mg^{2+} concentrations (Table 1) were observed at WHC2b (f_{UB} = 0.62) and WHC2c (f_{UB} = 0.32) suggesting possible mixing of Mg^{2+}—HCO_3^- fluids resulting in lower Ca^{2+}/Mg^{2+} ratios. Similar concentrations of Mg^{2+} and low Ca^{2+}/Mg^{2+} ratios were observed at TLE and WB (Table 1), suggesting possible incomplete or inactive serpentinization at these localities.

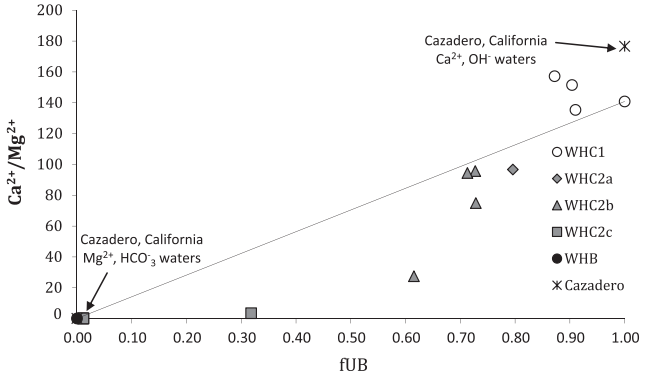

Fig. 5. Ca^{2+}/Mg^{2+} plotted versus the fraction of ultra basic water mixing with the conservative mixing line. Ca^{2+}/Mg^{2+} ratios increase with greater fraction of ultra basic water. Ca^{2+}/Mg^{2+} of waters from the Tablelands are plotted against Ca^{2+}/Mg^{2+} ratios of spring (Ca^{2+}/Mg^{2+} = 177) and meteoric water (Ca^{2+}/Mg^{2+} = 0.14) from another continental site of present-day serpentinization in Cazadero, California (Barnes et al., 1967). Error bars of Ca^{2+}/Mg^{2+} are ±10% and may appear smaller than the plotted symbol.

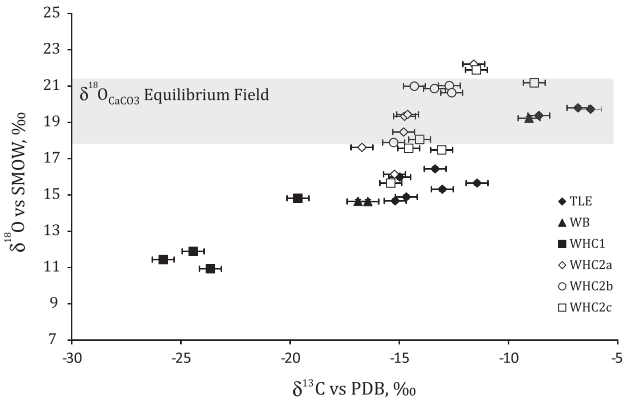

Fig. 6. $\delta^{18}O$ and $\delta^{13}C$ of travertine (filled symbols) and carbonate sediment (open symbols) from serpentinization sites plotted with the equilibrium field for $^{18}O_{CaCO3}$ (17.9–21.0‰) determined by O'Neil et al. (1969) corrected in Friedman and O'Neil (1977) assuming chemical precipitation of calcium carbonate in equilibrium with Tableland source waters. Error bars represent ±0.1‰ and ±0.5‰ for ^{18}O and ^{13}C respectively. Note that $\delta^{18}O$ bars are smaller than the plotted symbol.

3.4. Carbonate mineralogy and deposition

Carbonates have been observed to precipitate at the discharge points of ultra-basic springs emanating from altered ophiolites (Barnes and O'Neil, 1971). Carbonates in the form of travertine and sediment were found at ultra-basic springs discharging from serpentinized peridotite in the Tablelands. X-ray Diffraction (XRD) analyses of travertine and carbonate sediments from the Tablelands suggest the carbonates found at all sites primarily consist of calcite (>90%) with a lesser amount of aragonite (<10%).

The isotopic composition of carbonates can be used to understand the geochemical conditions under which the carbonates were deposited and can be used to interpret the inorganic carbon origin (Clark and Fritz, 1997). Stable carbon and oxygen isotope compositions (of $\delta^{13}C$ and $\delta^{18}O$) in travertine and carbonate sediment were determined (Fig. 6) and compared to the $\delta^{18}O$ of water and $\delta^{13}C$ of dissolved TIC (Table 2).

The large range in the $\delta^{13}C$ of the carbonates in this study (Fig. 6) has also been observed in other freshwater carbonates at sites of present-day serpentinization (O'Neil and Barnes, 1971; Clark et al., 1992). Carbon isotope fractionation during chemical precipitation of freshwater carbonates is dependent on the rate of carbonate precipitation, temperature of precipitation, and the carbonate species present; therefore, a large range in the $\delta^{13}C_{CaCO3}$ can be observed (Turner, 1982). During this process TIC provides carbon for carbonate precipitation. TIC is the sum of dissolved carbon species: $CO_{2\ (aq)}$, H_2CO_3, HCO_3^-, and CO_3^{2-}. In the ultra-basic springs at the Tablelands (pH > 10), the carbonate ion, CO_3^{2-}, is the predominant inorganic carbon species and can be assumed to make up most of the TIC composition. The enrichment factor between CO_3^{2-} and $CaCO_3$ is small (i.e. ~0.9‰ at 25 °C) (Mook, 1974). Therefore, it is not unexpected that the $\delta^{13}C$ composition of carbonates reflects the $\delta^{13}C$ composition of the TIC within roughly 1‰.

Since the $\delta^{13}C_{CaCO3}$ is largely influenced by the isotopic composition of the TIC, it is necessary to understand the origin of inorganic carbon that is contributing to the isotopic composition of the TIC pool. Different sources of inorganic carbon (i.e. CO_2) for carbonates can exist and contribute to the $\delta^{13}C_{TIC}$, thus providing a wide range of isotope compositions. Relative contributions of $CO_{2\ (g)}$ can be derived from the atmosphere ($\delta^{13}C \sim -7$‰) (Clark and Fritz, 1997); terrestrial organic matter ($\delta^{13}C \leqslant -24$‰) (Deines, 1980); marine organic matter ($\delta^{13}C \geqslant -23$‰); marine-carbonate ($\delta^{13}C \sim 0$‰) (Anderson and Arthur, 1983) and CO_2 from microbial methane oxidation ($\delta^{13}C \sim -54$ to -30‰, assuming a starting $\delta^{13}C$ methane of -60‰) (Whiticar, 1999). In addition to the isotopic composition of the initial CO_2, the $\delta^{18}C$ of carbonates is also influenced by the temperature-controlled fractionation between $CaCO_3$ and $CO_{2(g)}$. The initial $\delta^{13}C$ $CO_{2(g)}$ contributing to the formation of carbonates was determined using the equilibrium calcite–$CO_{2(g)}$ isotope fractionation ($\varepsilon_{Calcite-CO2(g)}$) relationship determined by Bottinga (1969) and the measured temperatures of the sampled spring fluids (Table 3). The calculated starting $\delta^{13}C_{CO2(g)}$ ranged from -36.2‰ to -27.1‰. The calculated $\delta^{13}C$ of the initial CO_2 is more depleted in ^{13}C compared to atmospheric CO_2 Calcite precipitation in equilibrium with $CO_{2\ (g)}$ is enriched in carbon by ~11‰, and aragonite by 12.8‰ (Rubinson, 1969). Additionally, the $\delta^{18}C$ of carbonates can be influenced by the temperature-controlled fractionation between $CaCO_3$ and CO_2. Using the measured temperatures of the sampled spring fluids, equilibrium calcite–$CO_{2(g)}$ isotope fractionations were calculated using the $\varepsilon_{Calcite-CO2(g)}$ relationship developed by Bottinga (1969) (Table 2). If the precipitation of the carbonates were simply due to atmospheric CO_2 dissolving into the water and precipitating, the $\delta^{13}C$ of the carbonates would be expected to be -19.0‰ to -17.4‰. Using calculated $\varepsilon_{Calcite-CO2(g)}$, starting $\delta^{13}C$ of $CO_{2(g)}$ was calculated (Table 2). Equilibrium fractionations ranged from 10.1 to 12.0 yielding starting $\delta^{13}C_{CO2(g)}$ from -36.2‰ to -27.1‰ suggesting, in addition to atmospheric CO_2 dissolution, there may be oxidation of terrestrial organic matter and/or methane contributing to the carbonates associated with the ultra-basic springs.

Table 2
Isotopic composition of total inorganic carbon, water, and carbonates.

Site	Measured $\delta^{13}C_{TIC}$ (‰)	Measured $\delta^{13}C_{CaCO3}$ (‰)	Measured $\delta^{18}O_{CaCO3}$ (‰)	Measured Avg. $\delta^{18}O_{H2O}$ (‰)	T_M (°C)	Calculated $\varepsilon_{Calcite-CO2(g)}$[a]	Calculated $\delta^{13}C_{CO2(g)}$ (‰)[b]	Calculated $\delta^{18}O_{CaCO3}$ (‰)[c]
WHC1	−30.6 to −28.2	−25.8 to −19.6	10.9–14.8	−9.5 (±0.1)	21.3–24.3	10.1–10.4	−36.2 to −35.9	19.0–19.7
WHC2a	−19.8 to −13.0	−16.7 to −11.6	16.1–22.2	−11.0 (±0.2)	10.5–15.5	11.1–11.7	−28.4 to −27.8	19.5–20.7
WHC2b	−19.2 to −12.5	−15.2 to −12.6	17.9–21.0	−10.8 (±0.3)	10.4–16.2	11.0–11.7	−26.9 to −26.2	19.5–20.9
WHC2c	−13.3 to −16.5	−15.4 to −8.8	15.7–21.9	−10.5 (±0.5)	11.3–17.2	10.9–11.6	−27.0 to −26.3	19.6–21.0
WB	−20.7 to −16.5	−16.7 to −9.9	14.6–19.2	−11.6 (±0.1)	10.0–19.9	10.6–11.8	−28.5 to −27.3	17.9–20.2
TLE	−15.5 to −9.9	−15.2 to −6.2	14.7–19.8	−12.3 (±0.1)	8.3–9.1	11.9–12.0	−27.2 to −27.1	19.7–19.9

T_M = Temperature measured, $\delta^{13}C$ reported versus PDB and $\delta^{18}O$ reported versus SMOW.

[a] Calculated equilibrium carbon enrichment between calcite and $CO_{2(g)}$ using fractionation equation: $1000 \ln \alpha = 1.435 \times 10^6/T^2 - 6.13$ (Bottinga, 1969).

[b] Calculated equilibrium $\delta^{13}C_{CO2\ (g)}$ using $\varepsilon_{calcite-CO2(g)}$ and measured $\delta^{13}C_{CaCO3}$.

[c] Calculated equilibrium carbonate oxygen isotope composition using fractionation equation: $1000 \ln \alpha = 2.78 \times 10^6/T^2 - 2.89$ (O'Neil et al., 1969; corrected in Friedman and O'Neil (1977)).

$\delta^{18}O$ of carbonates are influenced by the temperature-controlled fractionation between $CaCO_3$ and water, and the $\delta^{18}O$ of the water. The observed $\delta^{18}O_{CaCO3}$ for travertine and carbonate sediment ranged from 10.9‰ to 21.9‰ (Fig. 6). Using the measured isotopic compositions and temperatures of the sampled spring fluids, and calcite-water oxygen isotope fractionations (O'Neil et al., 1969), corrected in Friedman and O'Neil (1977), theoretical calcite $\delta^{18}O_{CaCO3}$ VSMOW values were calculated (Table 2). This isotopic fractionation assumes that the carbonates were precipitated in equilibrium with the water. The calculated equilibrium $\delta^{18}O_{CaCO3}$ values ranged from 17.9‰ to 21.0‰. The $\delta^{18}O_{CaCO3}$ data collected from WHC2b and WB fall within the calculated equilibrium $\delta^{18}O$ range based on the water isotopes, and temperature at the time of sampling. Data from TLE, WHC2a, and WHC2c only partially fall within the calculated equilibrium $\delta^{18}O$ range, where as data from WHC1 does not fall within the calculated equilibrium range. For the most part, $\delta^{18}O_{CaCO3}$ that are not well described by the equilibrium $\delta^{18}O$ range are more depleted in ^{18}O. A similar isotopic depletion in ^{18}O has been measured in travertine deposits and carbonate sediments at ultra-basic reducing springs at continental sites of serpentinization such as Cazadero, CA and the Oman ophiolite (O'Neil and Barnes, 1971; Clark et al., 1992). O'Neil and Barnes (1971) attributed this depletion in ^{18}O to the rapid precipitation of CO_2 in an alkaline solution where by two-thirds of the oxygen in the solid carbonate comes from the CO_2 and therefore isotopically depleted oxygen of $CaCO_3$ would have been expected.

3.5. Source of CH_4 and low molecular weight hydrocarbons in spring fluids

Dissolved hydrocarbon gases including: methane, ethane, propane, *n*-butane, *n*-pentane, and *n*-hexane were measured in ultra-basic reducing springs. Highest hydrocarbon concentrations were at the most reducing sites WHC2a and WHC2b (Table 3). Lesser amounts of dissolved hydrocarbon gases were measured at sites with greater mixing between the ultra-basic reducing groundwater and the surface freshwater (WHC2c) and at slow discharge rates (WHC1). In the latter case hydrocarbons may have been lost to the atmosphere before they could be sampled. In order to obtain a fresh spring water sample, all water was removed from WHC1 and the small depression in the travertine was allowed to fill again before the water was sampled. It was noted that the E_h became more positive while the pool was filling up, suggesting that the geochemistry of the water was changing very quickly in the presence of air. Therefore, hydrocarbons, inorganic carbon, and dissolved organic matter may have been partially or completely lost before sampling. At sites with the greatest amount of mixing, dissolved hydrocarbon gases were below detection (TLE and WB).

As a first approach, a Bernard plot (Fig. 7) was used to determine the primary source of CH_4 in the ultra-basic reducing springs. The, Bernard plot has been used previously to discriminate between microbial and thermogenic methane production (Bernard et al., 1977). Bernard et al. (1977) found that on a plot of $\delta^{13}C_{CH4}$ versus CH_4/C_{2+} (where C_{2+} is the sum of the concentrations of C_2, C_3, and C_4) that microbially produced methane has high CH_4/C_{2+} ratios (>400) and very negative $\delta^{13}C$ values (<−50‰) relative to thermogenic methane with lower CH_4/C_{2+} (<100) and more positive $\delta^{13}C$ values (>−50‰). Dissolved methane from the ultra-basic springs at the Tablelands plot in the thermogenic field suggesting that the primary source of methane is not microbial in these springs. This observation is consistent with initial microbiological studies of the Tablelands spring fluids, which have found a lack of significant contribution from biological methanogenesis (Brazelton et al., 2012). All methanogens are members of the Archaea, and attempts to detect archaeal 16S ribosomal RNA genes in Tablelands fluids via the polymerase chain reaction have failed. In contrast, bacterial 16S ribosomal RNA genes are readily detected (Brazelton et al., 2012). Furthermore, metagenomic sequences predicted to represent methanogens comprise only 0.2% of the full metagenomic dataset from WHC2b (Brazelton et al., 2012); data are available at http://metagenomics.anl.gov under dataset "WHC2B sff"). These predictions are based on automated sequence similarity algorithms, and none of the predicted sequences actually encode proteins directly involved in the methanogenesis pathway. In short, the available microbiological data indicate that if methanogens are present in WHC2b at all, they are extremely rare.

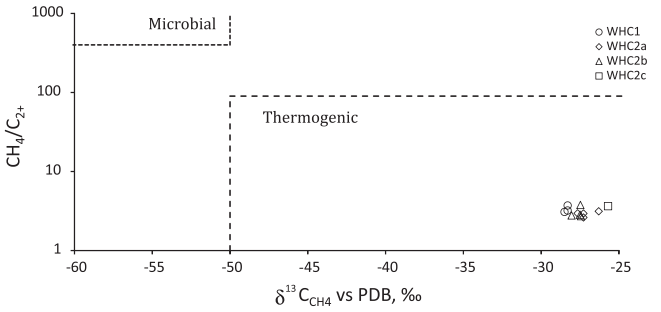

Fig. 7. Modified Bernard plot of $CH_4/[C_2 + C_3 + nC_4]$ versus $\delta^{13}C$ of methane from ultra-basic springs. Two distinct fields for microbially and thermogenically produced methane are plotted. Data points for hydrocarbon gases collected at the Tablelands fall within the thermogenic field.

The measured methane plots within a similar isotopic range (Fig. 7). However, one data point collected from WHC2c in August 2010 had an enriched value ($\delta^{13}C_{CH4} = -15.9$‰), where C_{2+} was below detection limit. This enriched CH_4 value may be evidence of methane oxidation occurring at WHC2c where there is O_2 present. Assuming a carbon isotopic signature of oxidized methane similar to that reported in June 2010 (−25.6‰), and uptake of the isotopically light carbon for metabolism, the left over carbon pool would be enriched in ^{13}C as observed at WHC2c from August 2010. Likewise, the TIC produced via oxidation will be depleted relative to

Table 3
Gaseous composition of spring waters.

	TLE	WHC2c	WHC2b	WHC2a	WHC1
H_2 (mg/L)	0.13–0.36	0.07–0.57	0.47–1.04	0.47–1.18	0.06
CH_4 (mg/L)	<d.l.	0.03–0.05	0.04–0.32	0.16–0.38	0.03–0.06
C_2H_6 (mg/L)	<d.l.	0.004–0.03	0.01–0.03	0.02–0.04	0.004–0.01
C_3H_8 (mg/L)	<d.l.	0.01–0.03	0.01–0.04	0.03–0.05	0.004–0.01
nC_4H_{10} (mg/L)	<d.l.	0.01	0.01–0.02	0.01–0.02	0.004
nC_5H_{12} (mg/L)	<d.l.	0.01	0.01	0.01–0.02	0.004
nC_6H_{14} (mg/L)	<d.l.	0.005–0.01	0.01–0.02	0.02–0.04	0.004–0.01
CH_4/C_{2+}	NA	0.68–3.65	2.78–3.78	2.62–3.14	3.08–3.72
$\delta^{13}C_{CH4}$(‰)	<d.l.	−15.9 to −26.3	−26.4 to −28.0	−26.4 to −27.7	−27.2 to −28.5

<d.l. = Less than detection limit, NA = not analyzed.

the carbon source, as was observed with a depleted $^{13}C_{TIC}$ (−17.3‰) sampled in August 2010. A decrease in CH_4 concentration and increase in TIC concentration was also observed in August 2010 (0.01 μg/L, 2.16 μg/L) as compared to June (0.03 μg/L, 1.73 μg/L) suggesting possible CH_4 uptake and CO_2 production from methane oxidation. During microbial oxidation the TIC would increase, and become depleted in $^{13}C_{TIC}$.

The methane measured may be thermogenic in origin. Thermogenic methane could be produced from the thermal alteration of the sedimentary organic matter underlying the Tablelands Ophiolite, and then migrated to the surface through cracks and fissures in the altered peridotite. Sedimentary organic matter most likely exists in the siliclastic marine sandstones from the Blow-me-Down Brook formation, siliclastic marine mélange from the Crolly Cove formation, and carbonate limestone from McKenzie's formation (see geologic map, Fig. 1). Therefore, a thermogenic origin of the methane must be considered; however, an abiogenic origin must also be considered.

Although an abiogenic field is not found on a Bernard plot, experimental and field studies have shown the CH_4/C_{2+} for abiogenic hydrocarbons (0.02–30) can overlap with the lower range of CH_4/C_{2+} ratios for thermogenic hydrocarbons, especially if mixing with thermogenic hydrocarbons (McCollom and Seewald, 2006; Taran et al., 2007, and references there in; McCollom et al., 2010). CH_4/C_{2+} ratios from the Tablelands springs (0.68–3.78) fall within this range. Therefore, the Bernard plot cannot discriminate between thermogenic and abiogenic sources of CH_4 within this range.

To distinguish between thermogenic and abiogenic origins of methane and higher molecular weight hydrocarbons, patterns of $\delta^{13}C$ and δD values of C_1–C_6 alkanes were considered. Thermogenic hydrocarbons have been shown to have a ^{13}C enrichment with increasing carbon number. This isotopic trend is attributed to kinetic isotopic effects where alkyl groups cleave from the source organic matter. The weaker ^{12}C–^{12}C bonds will break at a faster rate than the heavier ^{12}C–^{13}C bond (DesMarais et al., 1981). As a result of breaking the weaker ^{12}C–^{12}C bond, residual alkanes will be more enriched in the ^{13}C with increasing molecular mass. In contrast, it has been suggested that ethane can form abiogenically via a polymerization reaction demonstrating an isotopic depletion in ^{13}C and enrichment in D with respect to methane (Sherwood Lollar et al., 2002). In this polymerization reaction, the lighter isotopes ^{12}C–^{12}C will bond at a faster rate than the heavier and lighter isotopes ^{12}C–^{13}C, resulting in a depletion of ^{13}C of ethane compared to that of methane. In this study, the $\delta^{13}C$ of alkanes from WHC2a and WHC2b follow a general isotopic depletion of C_2–C_6 relative to CH_4 with increasing carbon number and a clear ^{13}C depletion between methane and ethane similar to other putative abiogenic hydrocarbons (Fig. 8). However, it must be noted that this ^{13}C depletion between methane and ethane is not consistently observed for abiogenic hydrocarbons (Taran et al., 2007). Sherwood Lollar et al. (2008) proposed that a sawtooth pattern, in this case a ^{13}C depletion between methane and ethane followed by a ^{13}C enrichment between ethane and propane, can be modeled assuming rapid abiogenic polymerized chain growth with negligible carbon isotope fractionation in the formation of C_{2+} compounds (Fig. 8). The Tablelands C_{2+} data is not well described by such a model suggesting that the carbon isotopic patterns observed at the Tablelands may be due to fractionation effects associated with secondary alteration processes such as oxidation or diffusion, or mixing of hydrocarbons from thermogenic and/or abiogenic sources.

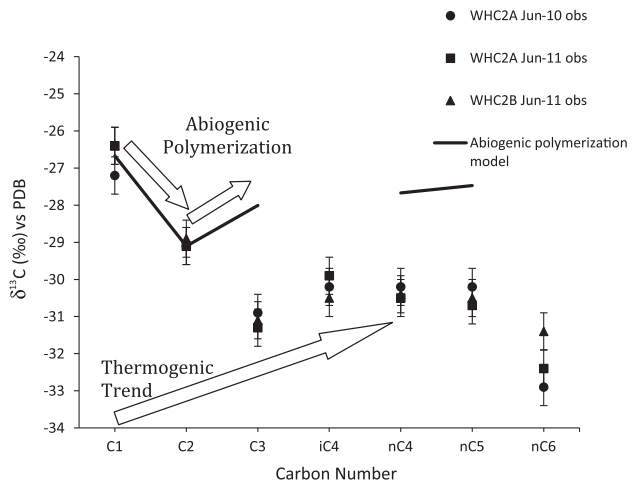

Fig. 8. Natural gas plot of $\delta^{13}C$ of hydrocarbon gases sampled at WHC2a, and WHC2b in June 2010, June 201. Error bars represent ±0.5‰ for $\delta^{13}C$. The block arrows represent general abiogenic and thermogenic isotopic trends. The solid line shows the predicted $\delta^{13}C$ values using an abiogenic polymerization model developed by Sherwood Lollar et al. (2008) using the following equations: $\delta^{13}C_{C2} = 1000 \ln \alpha + \delta^{13}C_{CH4}$ (Eq. (7)), $\delta^{13}C_{C3} = 0.33\delta^{13}C_{CH4} + 0.66\delta^{13}C_{C2}$ (Eq. (8)), $\delta^{13}C_{nC4} = 0.25\delta^{13}C_{CH4} + 0.75\delta^{13}C_{C3}$ (Eq. (9)), and $\delta^{13}C_{nC54} = 0.2\delta^{13}C_{CH4} + 0.8\delta^{13}C_{C4}$ (Eq. (10)), where $\alpha = (1000 + \delta^{13}C_{C2})/(1000 + \delta^{13}C_{CH4})$ (Eq. (11)). The initial input data ($\delta^{13}C_{CH4}$ and $\delta^{13}C_{C2}$) for the abiogenic polymerization model were the average carbon isotope values of methane and ethane measured at the Tablelands.

4. Implications and conclusions

Spatial variations in methane concentrations have been observed in the martian atmosphere suggesting the presence of localized source regions (Formisano et al., 2004; Mumma et al., 2009). This suggests that production and/or release of methane to the martian atmosphere may be related to the geology of the planet's surface or subsurface. Possible source regions include Nili Fossae and NE Syrtis Major where aqueous altered olivine-rich rocks are exposed (Hamilton and Christensen, 2005; Mumma et al., 2009; Ehlmann et al., 2010). At Nili Fossae Mg-carbonates and Mg-rich serpentines have also be found (Ehlmann et al., 2010), and calcium pyroxenes have been detected at Syrtis Major (Rogers and Christensen, 2007). The presence of carbonate and serpentine signatures at localized methane source regions suggests that serpentinization may have occurred in the past on Mars. Given the short residence time of methane, detected methane at source regions would suggest either recent serpentinization where liquid water would need to be present, possibly in the subsurface, or Noachian and trapped as methane clathrates in the subsurface, and/or polar ice being released in the subsurface (Mumma et al., 2009).

The Tablelands Ophiolite is an active site of serpentinization and a Mars analogue for the presence of altered olivine-rich ultramafic rocks with both carbonate and serpentine signatures. Meteoric water reacting with ultramafic peridotites at the Tablelands forms geochemically distinct ultra-basic and reducing springs. These springs have characteristic Ca^{2+} and Mg^{2+} ion ratios. Calcium-rich carbonate sediment and travertine deposits have been found in and around the ultra-basic springs. Isotopic analyses of carbonates suggest that carbonate sediment and travertine derived carbon from CO_3^{2-} and are precipitated in non-equilibrium with the atmosphere and fluids. Dissolved gases including hydrogen, methane, and low molecular weight alkanes (C_2–C_6) have been measured in ultra-basic springs. The primary source of methane sampled from the springs is not microbial, but either thermogenic or abiogenic in origin, or a mixture of both. Additional work is needed to distinguish between the two possible sources of hydrocarbons. One possible approach is to examine the stable isotope composition of hydrogen of the hydrocarbon gases to determine if they are abiogenic or thermogenic in origin (Sherwood Lollar et al., 2008). With the current Mars Science Laboratory rover, goals

to survey gases such as methane in the martian atmosphere, stable isotope and abundance analyses of gases can be applied to help provide information on the source of methane on Mars. Likewise, serpentinization at the Tablelands Ophiolite can be used as a mineralogical indicator to understand previous aqueous environment conditions and as a geochemical indicator to understand the conditions suitable for methane production on Earth and potentially on other ultramafic planetary bodies such as Mars.

Overall, key measurements on serpentinizing systems including aqueous geochemistry, carbonate mineralogy, and evidence of organic molecules can help in both interpreting data from MSL and planning future Mars exploration missions.

Acknowledgments

This study was supported in part by grants from the Canadian Space Agency (CSA) Canadian Analogue Research Network (CARN) and CSA's Field Investigations, Natural Sciences and Engineering Research Council (NSERC) Discovery Grant awarded to PI Morrill, NSERC Alexander Graham Bell Canada Graduate Scholarship, and MITACS Accelerate. We would like to acknowledge M. Wilson, M. Johnston, C. Earle, A. Rietze, H. Kavanagh with their help in the field, A. Pye and G. Van Biesen for their technical assistance in the lab, and N. Debond for the helpful comments on the manuscript. We would also like to thank the reviewers for their helpful comments on this manuscript.

References

Abrajano, T.A., Sturchio, N., Kennedy, B.M., Lyon, G.L., Muehlenbachs, K., Bohlke, J.K., 1990. Geochemistry of reduced gas related to serpentinization of the Zambales ophiolite, Philippines. Appl. Geochem. 5, 625–630.

Anderson, T.F., Arthur, M.A., 1983. Stable isotopes of oxygen and carbon and their application to sedimentologic and paleoenvironmental problems. Stable Isotopes Sediment. Geol. 10, 11–1151.

Atreya, S.K., Mahaffy, P.R., Wong, A.S., 2007. Methane and related trace species on Mars: Origin, loss, implications for life, and habitability. Planet. Space Sci. 55, 358–369.

Barnes, I., O'Neil, J.R., 1971. Calcium–magnesium carbonate solid solutions from Holocene conglomerate cements and travertines in the Coast Range of California. Geochim. Cosmochim. Acta 35, 699–717.

Barnes, I., LaMarche, V.C., Himmelberg, G., 1967. Geochemical evidence of present-day serpentinization. Science 156, 830–832.

Barnes, I., Oneil, J.R., Trescases, J.J., 1978. Present day serpentinization in New-Caledonia, Oman and Yugoslavia. Geochim. Cosmochim. Acta 42, 144–145.

Berger, A. R., Bouchard, A., Brookes, I. A., Grant, D. R., Hay, S. G., Stevens, R. K., Geology, Topography, and vegetation, Gros Morne National Park, Newfoundland; Geological Survey of Canada. 1992, pp. 54.

Bernard, B., Brooks, J.M., Sackett, W.M., A geochemical model for characterization of hydrocarbon gas sources in marine sediments. In: Offshore Technology Conference, Ninth, Houston, TX, 1977, pp. 435–438.

Blank, J.G. et al., 2009. An alkaline spring system within the Del Puerto Ophiolite (California, USA): A Mars analog site. Planet. Space Sci. 57, 533–540.

Boston, P.M., Ivanov, M.V., McKay, C.P., 1992. On the possibility of chemosynthetic ecosystems in subsurface habitats on Mars. Icarus 95, 300–308.

Bottinga, Y., 1969. Calculated fractionation factors for carbon and hydrogen isotope exchange in the system calcite–carbon dioxide–graphite–methane–hydrogen–water vapor. Geochim. Cosmochim. Acta 33, 49–64.

Boynton, W.V. et al., 2009. Evidence for calcium carbonate at the Mars Phoenix landing site. Science 325, 61–64.

Brazelton, W.J., Schrenk, M.O., Kelley, D.S., Baross, J.A., 2006. Methane- and sulfur metabolizing microbial communities dominate the Lost City hydrothermal field ecosystem. Appl. Environ. Microbiol. 72, 6257–6270.

Brazelton, W.J., Nelson, B., Schrenk, M.O., 2012. Metagenomic evidence for H_2 oxidation and H_2 production by serpentinite-hosted subsurface microbial communities. Frontiers in Extreme Microbiology: Deep Subsurface Microbiology 2 (Special Issue).

Chastain, B., 2007. Methane clathrate hydrates as a potential source for martian atmospheric methane. Planet. Space Sci. 55, 1246–1256.

Clark, I., Fritz, P., 1997. Environmental Isotopes in Hydrogeology. Lewis Publishers, New York.

Clark, I.D., Fontes, J.C., Fritz, P., 1992. Stable isotope disequilibria in travertine from high Ph waters – Laboratory investigations and field observations from Oman. Geochim. Cosmochim. Acta 56, 2041–2050.

Coleman, R.G., Keith, T.E., 1971. A chemical study of serpentinization-burro mountain, California. J. Petrol. 12, 311–328.

Craig, H., 1961. Isotopic variations in meteoric waters. Science 133, 1702–1703.

Deines, P., 1980. The isotopic composition of reduced organic carbon. In: Fritz, P., Fontes, J.-C. (Eds.), Handbook of Environmental Isotope Geochemistry. Elsevier, pp. 329–406.

DesMarais, D.J., Donchin, J.H., Nehring, N.L., Truesdell, A.H., 1981. Molecular carbon isotopic evidence for the origin of geothermal hydrocarbons. Nature 292, 826–828.

Ehlmann, B.L. et al., 2008. Orbital identification of carbonate-bearing rocks on Mars. Science 322, 1828–1832.

Ehlmann, B.L., Mustard, J.F., Murchie, S.L., 2010. Geologic setting of serpentine deposits on Mars. Geophys. Res. Lett. 37, L06201, http://dx.doi.org/10.1029/2010GL042596.

Elthon, D., 1991. Geochemical evidence for formation of the Bay of Islands Ophiolite above a subduction zone. Nature 354, 140–143.

Etiope, G., Schoell, M., Hosgörmezd, H., 2011. Abiotic methane flux from the Chimaera seep and Tekirova ophiolites (Turkey): Understanding gas exhalation from low temperature serpentinization and implications for Mars. Earth Planet. Sci. Lett. 310, 96–104.

Formisano, V., Atreya, S., Encrenaz, T., Ignatiev, N., Giuranna, M., 2004. Detection of methane in the atmosphere of Mars. Science 306, 1758–1761.

Friedman, I., O'Neil, J.R., 1977. Compilation of stable isotope fractionation factors of geochemical interest. In: Fleischer, M. (Ed.), Data of Geochemistry, U.S. Geological Survey Professional Paper 440-KK, sixth ed. U.S.G.S., Reston (VA).

Hamilton, V.E., Christensen, P.R., 2005. Evidence for extensive, olivine-rich bedrock on Mars. Geology 33, 433–436.

Hoefen, T.M., Clark, R.N., Bandfield, J.L., Smith, M.D., Pearl, J.C., Christensen, P.R., 2003. Discovery of olivine in the Nili Fossae region of Mars. Science 302, 627–630.

Holt, J.W. et al., 2008. Radar sounding evidence for buried glaciers in the southern mid-latitudes of Mars. Science 322, 1235–1238.

Kelley, D.S. et al., 2005. A serpentinite-hosted ecosystem: The lost city hydrothermal field. Science 307, 1428–1434.

Krasnopolsky, V.A., Maillard, J.P., Owen, T.C., 2004. Detection of methane in the martian atmosphere: Evidence for life? Icarus 172, 537–547.

Mahaffy, P., 2008. Exploration of the habitability of Mars: Development of analytical protocols for measurement of organic carbon on the 2009 Mars Science Laboratory. Space Sci. Rev. 135, 255–268.

Mahaffy, P., 2012. The sample analysis at Mars investigation and instrument suite. Space Sci. Rev. 135 (1–4), 1–78.

Max, M.D., Clifford, S.M., 2000. The state, potential distribution and biological implications of methane in the martian crust. J. Geophys. Res. 105, 4165–4171.

McAuliffe, C., 1971. GC determination of solutes by multiple phase equilibration. Chem. Technol. 1, 46–51.

McCollom, T.M., Seewald, J.S., 2006. Carbon isotope composition of organic compounds produced by abiotic synthesis under hydrothermal conditions. Earth Planet. Sci. Lett. 243, 74–84.

McCollom, T.M., Lollar, B.S., Lacrampe-Couloume, G., Seewald, J.S., 2010. The influence of carbon source on abiotic organic synthesis and carbon isotope fractionation under hydrothermal conditions. Geochim. Cosmochim. Acta 74, 2717–2740.

McEwen, A., 2011. Seasonal flows on warm martian slopes. Science 333, 740–743.

Mook, W.G., 1974. Carbon isotope fractionation between dissolved bicarbonate and gaseous carbon dioxide. Earth Planet. Sci. Lett. 22, 169–176.

Mumma, M.J. et al., 2009. Strong release of methane on Mars in northern summer 2003. Science 323, 1041–1045.

Mustard, J.F. et al., 2008. Hydrated silicate minerals on Mars observed by the Mars reconnaissance orbiter CRISM instrument. Nature 454, 305–309.

Niles, P.B., Boynton, W.V., Hoffman, J.H., Ming, D.W., Hamara, D., 2010. Stable isotope measurements of martian atmospheric CO_2 at the Phoenix landing site. Science 329, 1334–1337.

O'Neil, J.R., Barnes, I., 1971. Cl3 and 018 compositions in some fresh-water carbonates associated with ultramafic rocks and serpentinites: Western United States. Geochim. Cosmochim. Acta 35, 687–697.

O'Neil, J.R., Clayton, R.N., Mayeda, T.K., 1969. Oxygen isotope fractionation in divalent metal carbonates. J. Chem. Phys. 51, 5547–5558.

Oze, C., Sharma, M., 2007. Serpentinization and the inorganic synthesis of H_2 in planetary surfaces. Icarus 186, 557–561.

Quesnel, Y. et al., 2009. Serpentinization of the martian crust during Noachian. Earth Planet. Sci. Lett. 277, 184–193.

Rogers, A.D., Christensen, P.R., 2007. Surface mineralogy of martian low-albedo regions from MGS–TES data: Implications for upper crustal evolution and surface alteration. J. Geophys. Res. E: Planets 112, E01003. http://dx.doi.org/10.1029/2006JE002727, 18 PP.

Rubinson, M., 1969. Carbon-13 fractionation between aragonite and calcite. Geochim. Cosmochim. Acta 33, 997–1002.

Rudd, J.W.M., Hamilton, R.D., Campbell, N.E.R., 1974. Measurement of microbial oxidation of methane in lake water. Limnol. Oceanogr. 19, 519–524.

Schulte, M., Blake, D., Hoehler, T., McMcCollom, T., 2006. Serpentinization and its implications for life on the early Earth and Mars. Astrobiology 6, 364–376.

Schulz, H., 1999. Short history and present trends of Fischer–Tropsch synthesis. Appl. Catal. A: Gen. 186, 3–12.

Sherwood Lollar, B., Westgate, T.D., Ward, J.A., Slater, G.F., Lacrampe-Couloume, G., 2002. Abiogenic formation of gaseous alkanes in the Earth's crust as a minor source of global hydrocarbon reservoirs. Nature 416, 522–524.

Sherwood Lollar, B., Lacrampe-Couloume, G., Voglesonger, K., Onstott, T.C., Pratt, L.M., Slater, G.F., 2008. Isotopic signatures of CH_4 and higher hydrocarbon gases

from Precambrian Shield sites: A model for abiogenic polymerization of hydrocarbons. Geochim. Cosmochim. Acta 72, 4778–4795.
Sleep, N.H., Meibom, A., Fridriksson, T., Coleman, R.G., Bird, D.K., 2004. H_2-rich fluids from serpentinization: Geochemical and biotic implications. Proc. Natl. Acad. Sci. 101, 12818–12823.
Stevens, R.K., 1988. Ophiolite oddities: Preliminary notices if nephrite jade, Sr-aragonite, troilite, and hyperalkaline springs from Newfoundland. GAC MAC Joint Annual Meeting, St. John's, Newfoundland, 1988.
Suen, C.J., Frey, F.A., Malpas, J., 1979. Bay of Islands Ophiolite suite, Newfoundland: Petrologic and geochemical characteristics with emphasis on rare Earth element geochemistry. Earth Planet. Sci. Lett. 45, 337–348.
Taran, Y.A., Kliger, G.A., Sevastianov, V.S., 2007. Carbon isotope effects in the open-system Fischer–Tropsch synthesis. Geochim. Cosmochim. Acta 71, 4474–4487.
Turner, J.V., 1982. Kinetic fractionation of carbon-13 during calcium carbonate precipitation. Geochim. Cosmochim. Acta 46, 1183–1191.
Vance, S., Harnmeijer, J., Kimura, J., Hussmann, H., DeMartin, B., Brown, J.M., 2007. Hydrothermal systems in small ocean planets. Astrobiology 7, 987–1005.
Whiticar, M.J., 1999. Carbon and hydrogen isotope systematics of bacterial formation and oxidation of methane. Chem. Geol. 161, 291–314.